Research Article

# Environmentally Friendly Method of Assembly of Cardanol and Cholesterol into Nanostructures Using a Continuous Flow Microfluidic Device

Alessandra Zizzari,* Ermelinda Bloise, Elisabetta Perrone, Diego Romano Perinelli, Marc Schmutz, Valentina Arima, Giuseppe Mele,* and Luigi Carbone*

Read Online

ACCESS | Metrics & More | Article Recommendations | Supporting Information

**ABSTRACT:** This study shows a viable and straightforward microfluidic method of assembly of cardanol (CA) and cholesterol (CH) into amphiphile nanostructures obtained through a hydrodynamic focusing approach according to which an alcoholic solution of CA and CH is constrained within a two-dimensional lamina shape by two lateral streams of borate buffer solution. The process is performed within glass-made cross-shaped micro-sized fluidic chips specially designed to achieve a laminar regime. CA, distilled from the cashew nut shell liquid, is demonstrated as a surface-active molecule in borate buffer basic medium and when mixed with CH it produces versatile nanovesicles through an in-batch solvent-free process. Compared to this conventional method, the microfluidic route allows operating under continuous flows, with a reduced amount of reagents and at lower experimental temperatures, ensuring no waste formation and the achievement of size-monodisperse amphiphile nanostructures that do not need further steps of purification. Electron microscopy analyses demonstrate that upon increasing CH in the lipid mixture, a switchover from spherical CA micelles to CA/CH mixed closed vesicles occurs. Differential scanning microcalorimetry confirms the formation of vesicular structures and evidences the primary role of CH, which increasingly lowers the temperature of transition depending on its concentration.
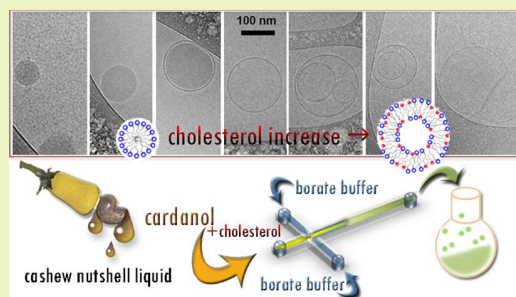
## INTRODUCTION

The application of the principles of green chemistry has become very important for designing sustainable chemical processes, especially if the latter are oriented to the reuse of waste materials from renewable resources for the production of high-value functional materials.[1] On the other hand, the development of miniaturized systems for the assembly of matter at the nanoscale through innovative environment-friendly processes may represent a relevant alternative route for the creation of materials that can show novel properties and functions and constitute a platform to investigate their mechanism of formation.[2] Relative to the conventional large-scale approaches, microscale technology leads to a larger number of advantages in terms of the lower amount of required reagents, time, and energy consumption, with also a consequent overall reduction of the waste generation process.[3−8] In this scenario, microfluidic technologies appear as a favorable and sustainable alternative to the traditional systems because the miniaturized dimensions and the high surface-area-to-volume ratios of microchannels represent ideal attributes for promoting a safe manipulation of the reagents, an increase in heat and mass transfer, an improved mixing

efficiency, and short diffusion paths.[8−10] These strategic advantages of microfluidic systems, over large-scale reactors provided real benefit in the pharmaceutical industry for the rapid, safe, and low-cost production processes,[11,12] as well as in green chromatographic separations,[13,14] chemical synthesis,[15−17] biocatalytic processes,[10] in biomedical devices and analytical or diagnostic tools.[7,18] For all these reasons, simple and low-cost microfluidic procedures are expected to progressively replace current batch and flow methods in favor of continuous and greener microscaled-down processes.[19,20] In particular, continuous flow microfluidics was already demonstrated as a technology for liposome production with tunable control over the physical properties of the end product, particularly in terms of liposome size distribution, allowing tunable and easy scale-up of vesicle synthesis.[21−23]

The production of precisely size-controlled nanovesicles, an ambitious program through conventional methods, is one of the essential topics for drug delivery and a means to improve nanomedicine performance, revolutionizing the life science field.

Among the different microfluidic techniques for liposome synthesis,[24−27] the microfluidic hydrodynamic focusing (MHF) device proved especially valid as it allows a fine regulation of the liposome size and dispersion achieved by tuning the flow rates of the solutions in the microchannels.[21,28] Moreover, a remarkable aspect from the perspective of the industries is that the MHF device offers the possibility to scale up the solution volume to be treated in the milliliter range, yet maintaining the peculiarities of the microscale.[9] This method sees that an alcoholic solution of lipids is hydrodynamically focused into a two-dimensional lamina by two adjacent tangentially flowing streams of buffered water (see the sketch in Figure 1a). Interdiffusion of water and alcohol molecules
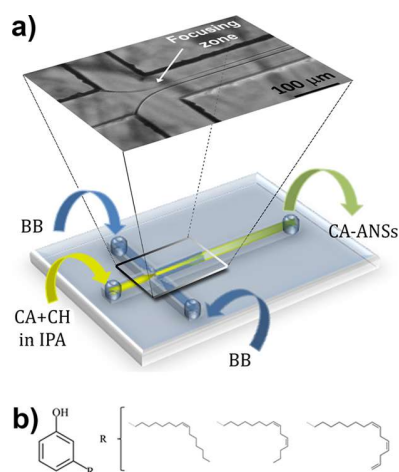


**Figure 1.** (a) Sketch of the microfluidic device (picture below) showing the injection geometry within microchannels. The picture on the top reports an optical image of the microchannels and the formed lamina as well as the focusing zone occurring at the crossing point of channels. (b) CA molecular structures.

occurs across the as-formed planar alcohol−water interfaces promoting an increase of the lipid concentration up to their solubility limit at which they precipitate, self-assembling into confined bilayered structures.[22,28] Mixing of reagents, based on a MHF mechanism, has proved to produce thermodynamically stable size-monodisperse lipid vesicles in the diameter range of sub 200 nm.[29]

Cardanol (CA) is a natural lipid waste obtained by distillation of the cashew nut shell liquid. It consists of a mixture of four phenolic compounds corresponding to the mono-, di-, and tri-unsaturated components and to the 3-*n*-pentadecylphenol, respectively (Figure 1b).[30,31] Its chemical features, such as a hydrophilic reactive phenolic group and a non-polar *meta* alkyl chain with non-isoprenoic cis double bonds, provide it an amphiphilic character and make it suitable for further chemical processing to develop CA-based derivatives.[32] Indeed, the hydrophilic−lipophilic balance value, according to the Griffin scale, is around 6 for the hydrogenated form of CA, likely because of the low polarity of the phenolic ring, therefore it is primarily soluble in organic solvents. Several examples in the literature have evidenced the

ability of CA: (i) to stabilize phospholipid-based liposome;[33] indeed, low values of the *n*-octanol−water partition coefficient (log $P$ = 3.54) indicate the favorable hydrophilic−lipophilic balance to accommodate CA molecules into a phospholipid bilayer; (ii) to be chemically engineered, via substitution in the phenolic ring or modification in the reactive hydroxyl group, to develop new breeds of CA-based amphiphiles,[34−37] which can be chemically driven to form stable nanoaggregates serving as soft templates for the growth of unique nanomaterials;[38−40] or (iii) to form bilayers by itself or in combination with cholesterol (CH).[41,42] This latter ability has shown to have a concentration-dependent role in promoting the cohesion of the membrane lipids,[43] to favor a liquid-ordered phase of the membrane,[44] to selectively modulate the fluidity of the membrane in either the polar part or in the hydrophobic region also,[45] and finally to affect the membrane permeability (or the drug release) to solutes.[45−47] Pure CA mixed with a minor amount of CH allowed forming stable nanovectors able to vehicle different kinds of molecules that can provide stabilizing,[30] antiproliferative, and antioxidant[48] effects and even function as a fluorescent tool for bioimaging.[49]

Here, for the first time, by the usage of MHF devices, we produced nanosized liposomal or micellar systems based on CA, or in combination with CH, substantially confirming the amphiphilic character of this compound,[41,50] particularly in basic media wherein it assumes an ionic character. By increasing the amount of CH in the lipid mixture, a system transition from spherical CA micelles to CA/CH mixed closed vesicles was demonstrated. We studied the effects of the flow parameters, temperature ($T$), and CH content in vesicle composition, on the vesicle structural properties [size, polydispersity index (PdI), and surface charge]. We demonstrated the sustainability of the microfluidic route not only to prove a smaller consumption of reagents and no waste production but also to evaluate the possibility to carry out the process under a continuous flow at $T$ lower than via the conventional (in-batch) methods,[49] with evident benefits in reduced costs and energy utilization. Very importantly, the smaller dimension and narrower size distribution of nanovesicles, resulting from the microfluidic approach, are relevant for biomedical applications. Indeed, vesicles ranging between 50 and 250 nm are injectable and represent promising drug delivery vector systems for personalized medicine.[51] In this view, consideration should be given to the well-documented added value provided by CA in terms of antioxidant activity,[52] therapeutic potential in the treatment of some diseases[53,54] as well as several other biological properties.[55−57] Ultimately, this offers many advantages because the amphiphilic CA-based nanostructures (hereafter abbreviated as CA-ANSs), in both the form of micelles and vesicles, by their very nature, could be used as therapeutic carriers themselves, without the need to load a drug as in the case of other liposomal delivery systems.[48]

## ■ EXPERIMENTAL SECTION

**Chemicals and Materials.** CA was kindly supplied by Oltremare S.r.l. and CH, KCl, H$_3$BO$_4$, and NaOH were purchased from Sigma-Aldrich (Steinheim, Germany) and used as received. Glass substrates were purchased from Telic (USA) and isopropyl alcohol (IPA), acetone, NaOH, HCl, NH$_4$F, and HF from Aldrich. The photoresist (AZ 9260) was purchased from MicroChemicals (Ulm, Germany). Chromium etchant solution was purchased from Poletto Aldo S.r.l., Noventa di Piave, Venice, Italy. Tubings (Tub FEP Blu 1/32 × 0.09) were purchased from IDEX HS (Germany) and TS10 glue was purchased from THORLABS (US).

**Preparation of the Solutions.** The borate buffer solution (pH = 9.0, BB, 50 ml) was prepared by mixing 30 mM $H_3BO_4$, 70 mM KCl, and 18 mM NaOH solutions in Ultrapure water delivered by a Zeneer UP 900 Human Corporation system.

Lipidic solutions were prepared by dissolving different molar ratios of CH and CA in IPA at room temperature (see Table S1) to obtain solutions with a fixed total lipid concentration of 0.9 mg/mL. Such concentration was optimized in previous studies for low solubility reagents to avoid clogging problems during microfluidic experiments.[21] To this end, the mixing solution was also filtered through a 0.45 $\mu$m filter.

**Fabrication of Microfluidic Chips.** The glass substrates covered by a thin chromium layer were cleaned with acetone and IPA. The cross-designed patterns (as shown in Figure 1a) with microchannels of a nominal width of 36 $\mu$m were transferred from a photomask (J.D. Photo-Tools Ltd., Oldham, Lancashire, UK) to the photoresist layer lying on the glass substrate, via UV light exposure. The photoresist was then developed, followed by the removal of the exposed chromium layer using the etchant solution, thus revealing the microchannels onto the glass substrate itself. Exposed glasses were then wet-etched with a buffered oxide etchant (solution prepared as reported by Zacheo et al.).[58] Wet etching procedure was performed by using a microwave reactor system, operating at a frequency of 2.45 GHz (Anton Paar Multiwave 3000, LabService Analytica S.r.l., Italy). Microchannels with a depth of about 40 $\mu$m have been produced. Next, inlet and outlet holes were drilled on the etched substrates before sealing microchannels by thermal bonding. Finally, capillary tubes were glued to the inlet and outlet holes.

**Microfluidic Approach for CA-ANS Production.** The setup for CA-ANSs production at a fixed temperature consisted of a single channel syringe pump (NE-1000 Multi-Phaser, QiS ProSense, The Netherlands) for the injection of CA/CH solution according to the ratios as reported in Table S1, a syringe pump with two channels (Ugo Basile, Biological Research Apparatus, model KDS270) for injection of the BB solution, an optical microscope with a high-resolution camera (Nikon Eclipse Ti), and a temperature-controlled optical stage to allow facile visualization of the laminar flow during heating. The chips were connected to the syringe pumps and fixed on the microscope heating stage set at different temperatures (22, 35, 50, 70 °C). The CA-ANS solutions were collected from the outlet in a vial. The flow rate ratios (FRRs, ratio of the volumetric flow of buffered water over lipid alcoholic solution) used for all the devices were 4, 6, 20, and 40 at the corresponding total volumetric flow $Q_t$ of 150, 42, 63, and 123 $\mu$L/min, respectively.

**Dynamic Light Scattering (DLS).** Size, PdI, and Z-potential of undiluted samples of CA-ANSs were determined by DLS and electrophoretic light scattering measurements using a Malvern Zetasizer Nano ZS90. The hydrodynamic diameter ($d$) was determined at 25 °C measuring the autocorrelation function at a 90° scattering angle. All the values reported are the average of three separate measurements ($D_{AV}$). The surface charge was determined at 25 °C from an average of three measurements. The voltage ramps were performed according to the DLS manufacturer's instructions.

**Surface Tension Measurements.** Air−water surface tension (mN/m) of different concentrations (0.08−0.5 mg/mL) of (i) CA in BB solution pH = 9, (ii) in BB solution/IPA (20:1 v/v), and (iii) BB solution/IPA (20:1 v/v) in the presence of 1 mg of CH was measured at 25 °C using a force tensiometer (DSC100, First Ten Angstroms, USA) according to the "Du Noüy ring" method. Data are reported as mean ± standard deviation of three measurements.

**Differential Scanning Microcalorimetry (Micro-DSC).** Calorimetric traces were recorded using a micro-DSC instrument (SETARAM III, France). 0.75 g of the sample was loaded in a Hastelloy vessel and the same amount of BB solution/IPA (20:1 v/v) was used as a reference. Heating scans were performed in the temperature range of 5−80 °C at a rate of 1 °C/min. Analyses were performed in triplicate. Transition temperatures and enthalpy values were calculated from the peak values and area.

**Transmission Electron Microscopy (TEM).** Positive stain-electron microscopy was employed to analyze the morphology of dilute dispersion of CA-ANSs.[59,60] Low-magnification TEM analyses were performed on a Jeol JEM-1011 electron microscope (Jeol Ltd., Akishima Tokyo, Japan) operating at 100 kV, equipped with a CCD camera ORIUS 831 from Gatan Inc. (Pleasanton, CA, USA). TEM samples were prepared by initially depositing a few drops of the liposome dispersions onto a carbon-coated copper grid and then, after almost 1 min, blotting off the sample with a filter paper. Afterward, a washing step was performed as follows: the TEM grid surface was made to touch a 25$\mu$L drop of 18.2 MΩ cm resistivity water deposited onto a parafilm and then, the excess of water was removed through a filter paper. This step was repeated twice. Finally, the staining procedure was accomplished by touching a 25$\mu$L drop of 1% (w/v) osmium tetroxide aqueous solution deposited onto a parafilm and removing the excess of solution as described above. Also this process was repeated twice. The grid was made to air-dry in a chemical hood.

**Cryogenic Transmission Electron Microscopy (Cryo-TEM).** A drop of 5 $\mu$L of the solution was applied to a copper grid covered with a carbon film made hydrophilic using an ELMO glow discharge device (Cordouan Technologies, France). The grid was placed in a home-made vitrification apparatus at 22 °C and 80% relative humidity before plunging into liquid ethane maintained at −190 °C by liquid nitrogen. The grid was mounted on a cryo holder (Gatan 626, USA) and observed using a Tecnai G2 microscope (FEI, The Netherlands) at 200 kV. Images were acquired using an Eagle slow-scan CCD camera (FEI).

## RESULTS AND DISCUSSION

In the following paragraphs, we provide details upon a novel method of production of CA-ANSs by using a MHF approach. The effectiveness of some parameters, such as injection flow rates, temperature, and CH/CA composition on the ANS assembly is reported. We also study the ANS size evolution by using DLS and investigate their morphology *via* electron microscopy.

Figure 1a shows a sketch of the characteristic setup suitably realized with a cross-shaped geometry to achieve a MHF regime. The micrometer-sized channels allow realization of laminar flows therein. The top image in Figure 1a shows a real optical microscope photograph of the alcoholic solution when thinned at the 90° crossing point by the two lateral flows of buffered solutions. As noted, the laminarity of lipid alcoholic solution is preserved for several millimeters length, up to the outlet zone.

**Influence of Flow Rates on ANS Size Distribution.** As mentioned above, a MHF device (Figure 1a) was selected to produce CA-ANSs in a controlled manner. Original system composition and experimental temperatures were chosen following the conventional in-batch method and adjusted accordingly.[49] A stream of organic solvent (IPA) containing the CH/CA mixture (0.6:1 molar ratio, solution 1 of Table S1) and a BB aqueous solution were injected, through programmable syringe pumps, respectively, within the central inlet microchannel and the two side channels. At the microchannels' crossing (*i.e.,* "focusing zone"), the solvent stream was focused into a narrow stream sheathed by the two adjacent flows of aqueous buffer (top picture in Figure 1a). Depending on the fluid focalization, the almost immediate interdiffusion of the species at the interface of the two phases converts the original surrounding alcoholic environment of the CH/CA into a water-rich medium. Therefore, the CH/CA molecules self-aggregate into short bilayer fragments because of the strong hydrophobic interactions between the alkyl chains and coalesce with each other until reaching a critical radius; hence, the fragments bend on themselves becoming vesicles, whose free energy is lower with respect to the fragments.[61] A 90-degree

crossing channel was preferred over lower angle intersections, as it was demonstrated that the shear forces occurring in this geometry improve hydrodynamic focusing effectiveness of the solvent stream with a consequent faster accomplishment of the interdiffusion of the two media[21] and then a production of smaller and size-monodisperse vesicles thereof.[29]

As well known, the MHF device allows to control the size of the amphiphile systems by modifying the total flow rate ($Q_t$) and the FRR in the side inlet channels (buffer solution) compared to the center inlet channel fed with lipids in alcohol. It was proved that $Q_t$, under high hydrodynamic focusing regimes, can slightly affect nanoparticles' size and their distribution.[21,23,29] We thus concentrated on the possibility to work under high focusing conditions, reducing the center channel stream width as much as possible and consequently the diffusion length for the reagents to be mixed.[28,29] Hence, as a first step, to prove the FRR efficacy on the size of ANSs, the solutions were injected at FRR values of 4 (120:30), 6 (36:6), 20 (60:3), and 40 (120:3). This latter value was the maximum FRR allowed by the fluidic network because higher values promoted the lateral BB solutions to flow back into the center inlet channel. Each experiment was carried out by fixing the heating plate of the microscope (onto which the chip was allocated) at 70 °C, the highest possible temperature before heavy effects of evaporation may occur. We observed certain stability of flows during the experiment that allowed us to measure (through optical microscope analysis) the width of the alcohol/lipid lamina resulting from the focusing flow conditions. As we can see in Figure S1, it stabilized reaching a plateau for FRR values greater than 20, indicating these as the highest possible hydrodynamic focusing conditions in our microfluidic system.

One mL of solution was collected for each experiment and analyzed by DLS in terms of dimensions and polydispersity. The resulting amphiphile structure diameters are reported in Figure 2a (magenta curve).

The trend of the curve shows that the size of the vesicles decreases by increasing the FRR until it reaches the plateau value (143 ± 57 nm) in correspondence of FRR = 20, then it slightly increases. As already reported for other types of amphiphile systems, the diffusive length along the focused lipid stream is the dominant factor controlling the vesicle size, so that higher FRR values result in smaller structures.[62] Indeed, a thinner organic lamina provided a faster water and alcohol interdiffusion along the stream width and therefore a more efficient mixing, the latter a fundamental condition for producing smaller ANSs in the laminar flow regime.[21] In particular, at low flow ratios, the size decreased sharply according to small FRR increases. On the contrary, for relatively higher FRR (in our case above 20) the smaller changes in the central stream width (see Table S2) led consequently to much smaller diameter changes.[63,64] A FRR increase reduced the lamina by more than half, so the alcohol stream width decreased by 61% upon incrementing FRR from 4 to 6; on the contrary, it remained unchanged for FRR increase above 20, thus resulting in very small size variations (Figure 2a, magenta curve). In the view of lamina thickening/thinning and successive concentration/dilution of central lipid solution, another evident factor to be considered is the larger extent of removal of IPA occurring at higher FRRs by means of extreme lateral BB aqueous streams, which can straightforwardly contribute to promoting a loss of solubility of lipid molecules.
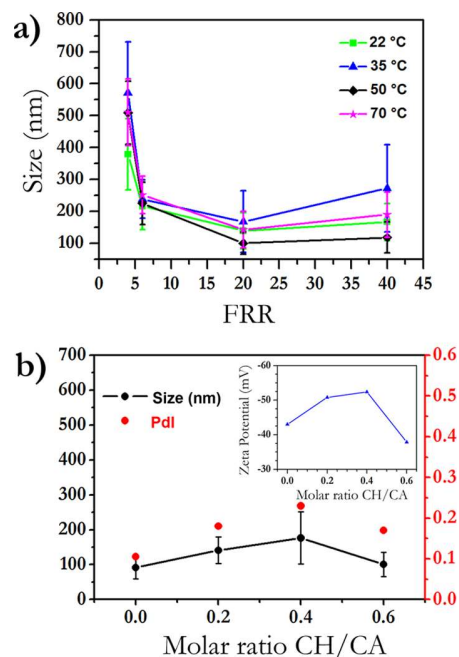


**Figure 2.** Results of microfluidic experiments. (a) Representative curves of the CA-ANS hydrodynamic size evolution as a function of FRR obtained by flowing solution 1 (CH/CA = 0.6:1 molar ratio) of Table S1 from the central inlet. Each experiment was performed by varying the FRR at a fixed temperature ($T$). (b) CA-ANS hydrodynamic size and their relative PdI trend depending on the CH/CA molar ratio. The experiments were performed at FRR = 20 and $T$ = 50 °C. In the inset, the CH/CA molar ratio dependence of the Z-potential is shown. The sizes reported in both pictures were achieved by DLS measurements.

The particle size uniformity was ascertained through PdI determination, defined, in the assumption of a Gaussian distribution, as the variance of the vesicle size distribution normalized by the square of average particle size.[65] The literature has established that as the FRR increases, the size distribution becomes less dispersed.[28] For the ANSs produced in this study, dispersity was found to vary with FRRs leading to a curve trend with a minimum PdI value of 0.05 at FRR 6 (data not shown). For the other FRRs, polydispersity values in the mid-range between 0.16 and 0.32 were found. A size distribution very sensitive to FRR variations demonstrated that even small changes in flow conditions and composition during ANS synthesis can have an impact on the PdI value. This phenomenon was justified by Jahn and co-workers, accounting for a mechanism of disassembly—reassembly of liposomes that move along the channel, undergoing the fluid streamlines, through zones with an alcohol concentration above or below the critical one.[28]

Compared to the in-batch approach,[49] the microfluidic route allowed producing size-monodisperse ANSs of different dimensions according to the FRRs, without further post-production size separation steps required. This proved to be beneficial in the perspective of investigating the influence of several other physico-chemical process variables such as temperature or system composition.

**Effects of Temperature.** It is known that the temperature affects the liposome size by changing the membrane elasticity, which is much larger in work conditions close to or below the gel-to-liquid crystalline phase transition temperature ($T_m$), so
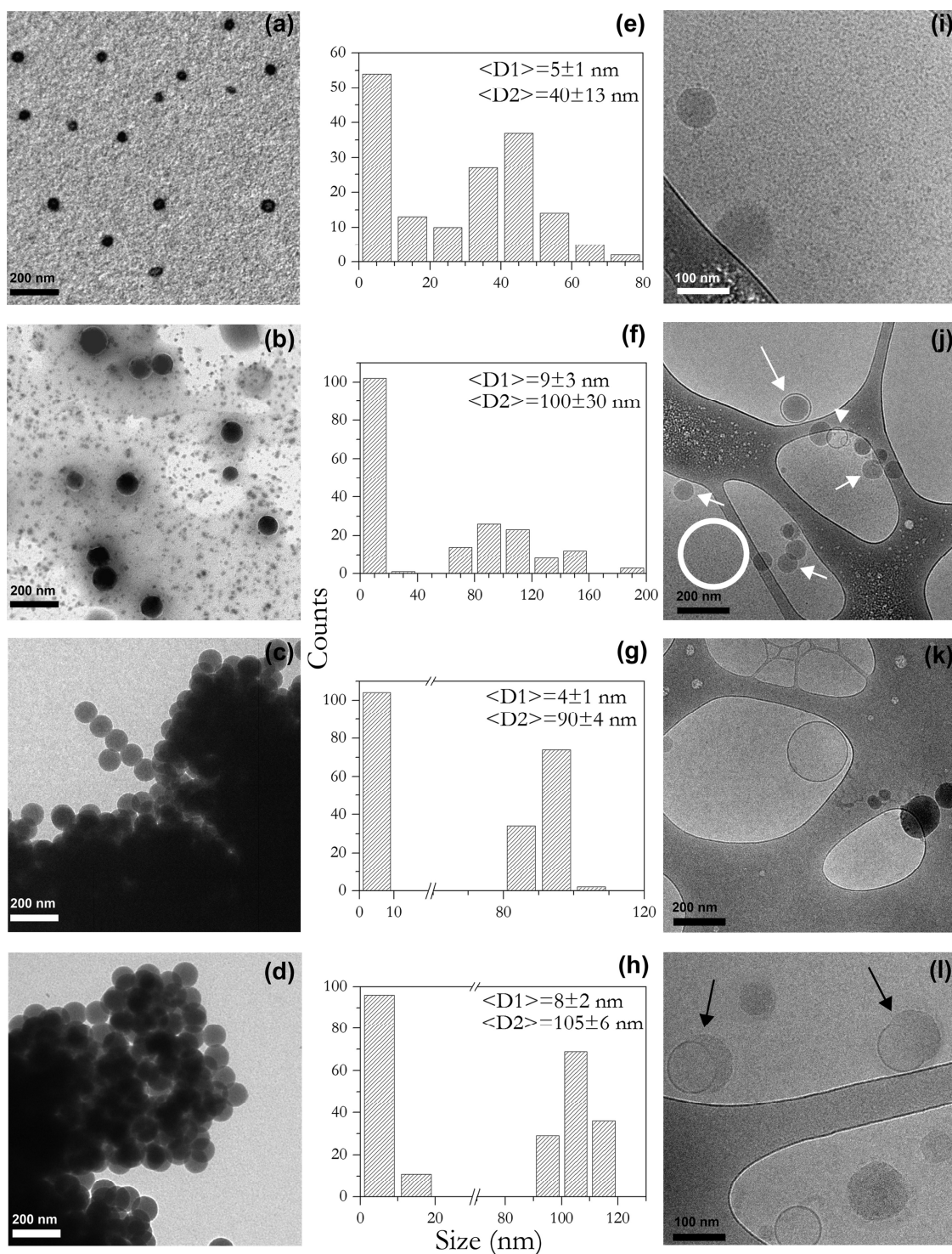
**Figure 3.** Low-magnification electron micrographs of CA/CH-based nanosized lipid aggregates. Bright-field TEM analysis of positively stained soft nanostructures of samples obtained with: (a) pure CA; (b) CA/CH = 1:0.2; (c) CA/CH = 1:0.4; and (d) CA/CH = 1:0.6 molar ratios. Pictures (e−h) report diameter size distribution histograms of each sample, obtained via TEM image statistic analysis. Micrographs (i−l) show cryo-TEM images of the same samples.

that larger liposomes are formed. On the contrary, according to the theory, smaller vesicles are produced working above the $T_m$ and, moreover, a much smaller temperature-dependence of size in a far above the $T_m$ condition occurs, due to a membrane elasticity modulus being relatively constant.[62,66] Hence, the $T$ dependence of the process of lipid assembly was evaluated as

well. Experiments were performed by placing a heater in contact with the chip at 50, 35, and 22 °C, and, for each of them, different FRRs (4, 6, 20, and 40) were explored as already done at 70 °C. The results are summarized in Figure 2a. With the only exception of outcomes observed at very high FRRs, the temperature does not show a significant effect on the

vesicle size. Indeed, the curves trend (green, blue, and black for 22, 35, and 50 °C, respectively) looks remarkably similar to the 70 °C one, as also the organic lamina behavior (Table S2). Thus, on the whole, it was observed that a progressive decrease of the ANS dimensions with FRR increase takes place, until to a plateau region, as typically happens for MHF architecture.[22,67] As regards to size uniformity, we can make similar considerations as those for 70 °C experiments. The PdI value of our nanosystems for each temperature was always in the mid-range ≤ 0.2 for all FRRs tested (data not shown). Because of the above-outlined results relating to FRR- and *T*-dependence, all other experiments carried out hereinafter were done at 50 °C and FRR = 20. Operative reasons primarily related to the employment of *T* and of FRR conditions able to provide sizes lower than 200 nm motivated this choice and this was corroborated by the outcomes provided by the micro-DSC measurements according to which an endothermic peak appears in the temperature range 30−55 °C (see below). Such experimental setting resulted largely being more accessible when compared to the procedure in-batch,[49] which, contrarily to the microfluidic route, requires two 90 °C steps to ensure the optimal solvent-free mixture of the pure components, followed by a 60 °C sonication and centrifugation to separate the smaller nanostructures from the larger ones.

**Effects of CH.** As large amounts of CA were expected to increase the drug properties of the amphiphile systems, a further parameter we investigated was the effect of CH/CA composition on the size of ANSs. It is well known that CH is a typical biocompatible lipidic component of liposomal systems and plays a strategic role in liposome composition. In the case of phospholipid-based systems, it increases the packing of the bilayer, changing its elasticity modulus and therefore the vesicle size,[62] its fluidity as well as the passive drug permeability.[46] In this view, in addition to the solution already studied (*i.e.*, CH/CA, 0.6:1, with the reference to the in-batch method), CH was mixed with CA in other different proportions (0:1, 0.2:1, and 0.4:1), keeping constant the total concentration (0.9 mg/mL). These mixtures were always studied at FRR = 20 and at 50 °C.

Figure 2b evidences very poor CH dependence of the ANS dimensions. In particular, in all CH-based examples, the sizes of the lipidic structures hovered around 100 nm, unlike the sample made by pure CA, which in fact exhibited hydrodynamic dimensions a little lower, whereas the PdIs extended between 0.11 and 0.18 suggesting complete independence on the CH amount of the size dispersity (see also Figure S2). In a similar manner, the addition of nonionic CH imperceptibly affected the surface charge of the ANSs, promoting a limited variability of the Z-potential values in the range between −40 and −50 mV. The amphipathic nonionic CH molecules share the interface with the negatively charged CA, which exposes its alkyl phenate form at the working pHs of buffer borate (inset Figure 2b) operating as an anionic surfactant-like molecule, therefore. The first addition of CH promoted an increase of the Z-potential as the system started to form larger particles, as later demonstrated by TEM analysis also, thereafter followed by a surface charge reduction caused by larger incorporations of nonionic CH at the interface and its screening effect toward anionic CA.[68] The samples stored at room temperature showed stability over time. The sizes evaluated via DLS after 4 months established variations in the range of 7% (data not reported), suggesting certain stability in solution and a scarce tendency to aggregate. Correlograms as shown in Figure S2

confirm the mid-range polydispersity and the lack of large particles or aggregates, this latter corroborated by the flatness of the baseline.

**Transmission Electron Microscopy.** The ANS morphology and size were also investigated by TEM analysis. The outcomes are summarized in Figure 3. The left column in the figure reports the bright-field TEM micrographs of the four samples produced by changing the CH/CA molar ratio. Synthesis results suggest that the lack of CH in the growth mixture does not contribute to an important enlargement of the ANSs. Indeed, spherical particles as large as 40 nm were observed (Figure 3a,e). Because of the osmium tetroxide positive staining, the soft nanoparticles appeared as strongly dark-colored. The CH addition, on the contrary, promoted the formation of larger spherical lipid nanoparticles of up to 100 nm (Figure 3b−d), nevertheless without showing a significant CH dependence thus confirming the DLS results. Interestingly, TEM investigations revealed for each sample the presence of another characteristic very small size fraction: histograms in Figure 3e−h and Figure S3 detail it distinctly. In all cases, dimensions of the order of 4−8 nm were detected. We hypothesize that the formation of these small nanosized structures may be attributed to the precipitation of lipid aggregates occurring because of the large increase of the water phase, as fast mixing with IPA changes the total polarity. Whether TEM could display the size and the morphology of the ANSs, it could not discriminate between the character of the amphiphile structures, that is, whether micellar (lipid monolayered spherical systems) or vesicular (lipid bilayered spherical systems).

Cryo-TEM analyses were performed as shown in Figure 3i−l. In detail, when CA was the only lipid agent, two different sizes of ANSs were formed, a larger one imaged in Figure 3i showing a diffuse interface and small spherical micelles representing most of the material. The latter has the tendency to form diffuse large aggregates. The sharp contrast evidenced the micellar habit of those structures (lipid particles). Apart from one liposome reported in Figure S4a (first picture), possible vesicles were not detected in this sample. The addition of CH in a molar ratio CH/CA = 0.2/1 promoted the growth of very regular ANSs presenting a dense core (short arrows) and a few liposomes (arrowhead) (Figure 3j) and also of some interesting structures made by a dense core surrounded by a membrane (long arrow) (Figures 3j and S4b). There are still some micelles seen in the background (circle). The observed liposomes present a typical bilayered structure of their membrane (seen in Figure S4b). Upon increasing the molar ratio CH/CA to 0.4/1, the system exhibited mainly liposomes relative to micelles (see Figures 3k and S4c). A similar trend was confirmed also for molar ratio CH/CA = 0.6/1. In this case, a larger density of liposomes was identified as well as Janus-like particles (arrow in Figure 3l). These Janus particles could be an intermediate structure between the dense particles shown in Figure 3j (white short arrow) and the liposome, the dense part acting as a reservoir for CA before interacting with CH and forming a bilayer (see Figures 3l and S4d).

Relative to the progressive addition of CH, cryo-TEM evidenced a net system phase transition from CA-based spherical micelles exhibiting rather small diameters to an environment displaying a large density of closed spherical vesicles made by CH and CA. At a moderate amount of CH, the coexistence of micellar and vesicular nanostructures is observed. The incorporation of CH promoted changes in the

radius of curvature of those structures and very large inclusions of CH were necessary (37% of moles) to observe most bilayered particles.

Taking into account the lipid molecular shape to model a membrane at the interface, it is recognized that the transition from micelles to vesicles matches with a change of the dimensionless lipid packing parameter, $S$, given by $S = V/al$, where $V$ represents the volume of the alkyl chain and $a$ and $l$ express the cross-sectional area of the head group and the length of the alkyl chain, respectively. The packing parameter provides a general indication of the lipid shape at the interface and of the architecture of the aggregates, thereof. When it is <1/3, its conical shape favors the formation of spherical micelles (whether the amphiphile concentration exceeds the critical micelle concentration) as a result of the side-by-side packing. The formation of vesicles occurs when $S > 1/2$, however being <1. In this case, the amphiphilic molecule takes a shape more similar to a cylinder, thus the side-by-side disposal generates bilayers that allow allocating more molecules at the interface.[69] Our experimental evidence suggests that nonionic CH promotes the transition from micelles to vesicles as, because of the additivity of the packing parameters of the lipids,[70] and placing itself at the interface, contributes to enlarging the volume of the hydrophobic part of CA favoring in this a proper change of the amphiphilic shape from conical to cylindrical. Indeed, to a larger amount of CH available at the interface corresponds an important buildup of vesicles relative to micelles. The literature has identified in the case of phospholipid/CH bilayers an important CH amount-dependent increase of the electron density of the phospholipid tail region due to CH ring structure localized in that portion (hydrophobic) of area.[68] In this view, steric encumbrance rendered by the alkyl chain unsaturation of CA contributes further, expanding therefore the hydrophobic $V$ of the packing parameter. On the other hand, the widespread presence of CH at the interface (without significantly changing the total number of molecules in the solutions) in different percentages allows screening of the negative charges of CA. The lateral diffusion of molecules at the interface decreases upon increasing the content of CH and the amount and location of free space is reduced.[68] For the reasons above detailed, the presence of CH at the interface meaningfully alters the packing of CA molecules facilitating the micelle-to-vesicle changeover and a CH concentration-dependent commensurate formation of vesicles.

**Surface Tension and Micro-DSC.** The surface properties of CA in the buffer and in the presence of CH were evaluated via force tensiometry analyses. Figure 4a summarizes the air–water surface tension values obtained by changing the concentration of CA from 0.08 to 0.5 mg/mL in different media: pure BB, BB/IPA (20:1 v/v), and BB/IPA (20:1 v/v) + 1 mg of CH. At all conditions, CA was able to decrease the surface tension as a function of its concentration, thereby behaving as a surface-active molecule. The extent of the surface tension decrease for any concentration of CA depends upon the characteristic of the media. Indeed, the measured surface tension values for pure BB and BB/IPA were different, being 72.18 ± 0.06 and 51.34 ± 0.09 mN/m, respectively. The absolute surface tension values of solutions at any CA concentration were higher in BB than in BB/IPA solution. On the contrary, the relative variation of surface tension between that of pure solvent and of the highest tested concentration of CA (0.5 mg/mL), named $\Delta_{S0-S0.5}$, was more
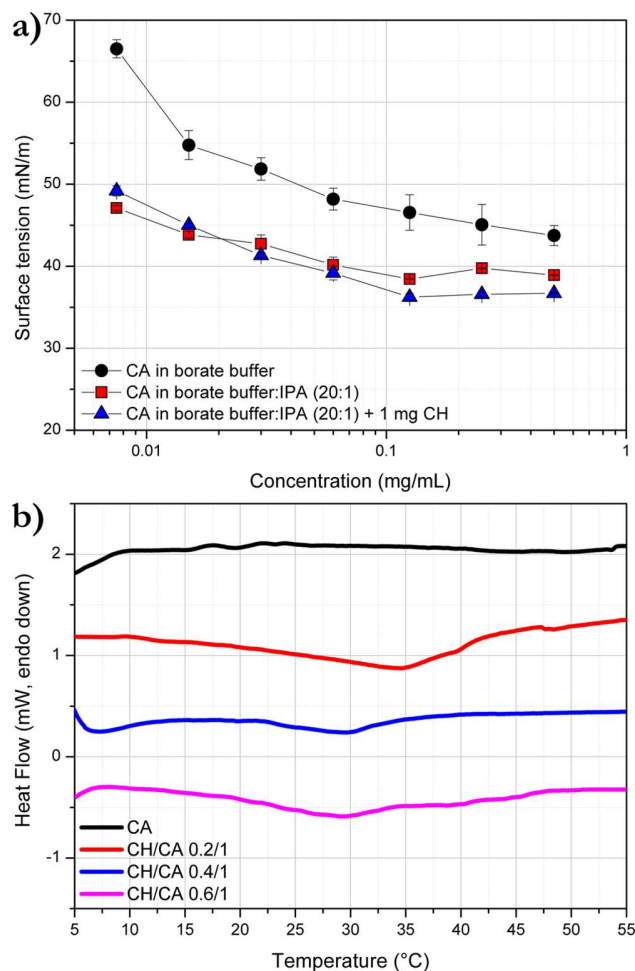
**Figure 4.** Surface tension and microcalorimetry measurements. (a) Surface tension (mN/m) vs concentration (mg/mL) of CA in BB pH = 9, BB/IPA (20:1 v/v), and BB/IPA (20:1 v/v) + 1 mg of CH. (b) Micro-DSC traces of CA and CH/CA mixtures at different molar ratios in BB/IPA (20:1 v/v).

pronounced in BB than in BB/IPA, being 28.44 and 12.43 mN/m, respectively. The presence of CH does not influence markedly the surface properties of CA, being the surface tension values measured for CA alone comparable to those in the presence of CH, as well as the calculated $\Delta_{S0-S0.5}$ values (12.43 mN/m vs 14.64 mN/m, respectively). The surface-active role of IPA is also clear, without significantly changing the viscosity of the system at the operative concentrations. As a co-surfactant and because of its miscibility with water in all proportions, IPA is expected to decrease the interfacial tension between both solvents and significantly facilitate the interdiffusion, thereby enhancing the mass diffusivity and the rates of formation of the self-assembled ANSs. Additionally, whether or not IPA may be placed at the interface mainly interacting with the polar heads of lipids and surfactants is an outcome that cannot be ruled out. However, we consider this view less plausible due to the very large amounts of water, even at low FRRs (IPA mole fraction < 0.055 at FRR = 4), that is supposed to perfectly solubilize (and solvate) single molecules of IPA.[71] At FRR = 20, the FRR employed to investigate the CH effect, the IPA volume results even < 5% (IPA mole fraction < 0.012).

Microcalorimetry enables the characterization of the thermal behavior of CA and CH/CA dispersions. The main detectable transitions are broad endothermic events in the temperature range between 15 and 55 °C, in which the mean transition temperature can be calculated from the peak value of the micro-DSC trace and the transition enthalpy (J/g of dispersion) from the associated area (Figure 4b). Thermal transitions are more evident for CH/CA samples at different ratios (CH/CA 0.2:1, 0.4:1, and 0.6:1) than for CA alone dispersion. The calculated values are 35.2 ± 4.2 °C and 0.294 ± 0.012 J/g for CH/CA 0.2/1 sample; 30.3 ± 2.8 °C and 0.136 ± 0.024 J/g for CH/CA 0.4/1 sample; and 30.0 ± 2.5 °C and 0.118 ± 0.021 J/g for CH/CA 0.6/1 sample, whereas an endothermic event associated with much lower energy is observed for CA alone (transition temperature 43.6 ± 0.5 °C and 0.014 ± 0.008 J/g). The presence of CH affects both the transition temperature and the associated energy. Indeed, CH determines a marked decrease in the transition temperature (from ~44 to ~30 °C) and a remarkable increase of enthalpy (from ~0.015 to ~0.300 J/g). The formation of nanovesicles is confirmed by the presence of a main thermal transition that is always preceded by some other pre-transitions (see Table S3), significantly favored by the addition of CH that, in accordance with TEM data, stabilizes the formation of vesicles (in place of micelles) and lowers the temperature at which these nanostructures form. This confirms the very large size variability observed at temperatures as low as 22 °C (Figure 2a) and the optimum choice to operate at temperatures in the range of 35−50 °C.

## CONCLUSIONS

Continuous flow microfluidics operating in a laminar regime is proposed as an alternative method to prepare amphiphile nanostructures based upon CA, a lipid mixture distilled by the cashew nut shell liquid, which also shows surface-active properties in its anionic form. At different thermal conditions, spherical micelles consisting of pure charged CA are formed. The incorporation of a lipid, CH in this case, favors a change in the form of assembly promoting the condensation of CH-stabilized closed vesicles and their extent of formation is accordingly related to the amount of CH. This trend exhibited by the system anionic CA−CH is perfectly consistent with the conventional three-stage framework of surfactant−lipid assemblies according to which when only the surfactant is present in the reaction mixture, CA herein, micelles are formed. The incorporation of a lipid, CH in our case, promotes the existence of mixed micelles, whereas the progressive addition of lipids stabilizes the formation of a larger amount of vesicles.[72,73] The CH-assisted micelle-to-vesicle changeover is read in the light of the geometric packing, a parameter that takes under consideration the interfacial mean curvature. The interaction of the lipid alters, according to its content, the original molecular shape of the anionic CA surfactant, given that both reagents set at the interface.

The experimental approach contributes to stabilizing the formation of those amphiphile structures, indeed, the variation of solubility following the water and IPA reciprocal interdiffusion during continuous flow microfluidics provides the energy to the system for the condensation of a new phase.[74] Only viscous forces regulate the laminar regime, thus the lack of turbulence makes the diffusion process the only mechanism of mass transfer, significantly enhanced at the microscale. The hydrodynamic focusing approach allows smaller consumption of reagents, limited waste production, and to carry out the process at a temperature lower than via the conventional methods because of the large heat transfer. By optimizing flow and temperature conditions, nanostructures as large as 100 nm or smaller are obtained. FRR results as a critical attribute to indirectly manipulate the concentration of reagents within each stream and therefore to change the conditions of growth.

The development of amphiphile-based green nanosystems obtained via sustainable practices tackles two important challenges of the scientific community: (i) to solve the issue of "green choices", a moral imperative of Chemistry and Engineering sectors and (ii) to provide appealing support to the personalized medicine that could satisfy the persistent demand of innovative therapeutic models in the healthcare sector.

## ASSOCIATED CONTENT

### Ⓢ Supporting Information

The Supporting Information is available free of charge at https://pubs.acs.org/doi/10.1021/acssuschemeng.2c01554.

CH-to-CA molar ratios as employed in each experiments; plot of the width of the alcohol/lipid lamina resulting from the focusing flow conditions as a function of FRR; width of the alcohol/lipid lamina resulting from the focusing flow conditions at different FRR and T; DLS size data; low-magnification TEM and cryo-TEM analyses; and micro-DSC analysis (PDF)

## AUTHOR INFORMATION

### Corresponding Authors

**Alessandra Zizzari** − *CNR NANOTEC—Institute of Nanotechnology, University of Salento, 73100 Lecce, Italy;* ⓘ orcid.org/0000-0002-9651-7922; Phone: 00 39 (0)832-3-19827; Email: alessandra.zizzari@unisalento.it

**Giuseppe Mele** − *Department of Engineering for Innovation, University of Salento, 73100 Lecce, Italy;* ⓘ orcid.org/0000-0002-6684-990X; Phone: 00 39 (0)832-297281; Email: giuseppe.mele@unisalento.it

**Luigi Carbone** − *CNR NANOTEC—Institute of Nanotechnology, University of Salento, 73100 Lecce, Italy;* ⓘ orcid.org/0000-0002-1369-6890; Phone: 00 39 (0)832-3-19819; Email: luigi.carbone@nanotec.cnr.it

### Authors

**Ermelinda Bloise** − *Department of Engineering for Innovation, University of Salento, 73100 Lecce, Italy*

**Elisabetta Perrone** − *CNR NANOTEC—Institute of Nanotechnology, University of Salento, 73100 Lecce, Italy*

**Diego Romano Perinelli** − *Chemistry Interdisciplinary Project (CHIP), School of Pharmacy, University of Camerino, 62032 Camerino, Italy;* ⓘ orcid.org/0000-0002-7686-4150

**Marc Schmutz** − *Université de Strasbourg-CNRS-Institut Charles Sadron UPR22, 67034 Strasbourg, France*

**Valentina Arima** − *CNR NANOTEC—Institute of Nanotechnology, University of Salento, 73100 Lecce, Italy*

Complete contact information is available at:
https://pubs.acs.org/10.1021/acssuschemeng.2c01554

### Author Contributions

A.Z. and E.B. contributed equally. A.Z., V.A., G.M., and L.C. conceived and designed the experiments. A.Z., E.B., and E.P.

pubs.acs.org/journal/ascecg

carried out the experiments. D.R.P. performed measurements of surface tension and micro-DSC. M.S. performed cryo-TEM analysis. L.C. performed TEM analysis. E.B. and G.M. contributed to cardanol. A.Z., V.A., and L.C. analyzed the data. A.Z., G.M., and L.C. wrote and reviewed the manuscript with the contributions of all authors. All authors have given approval to the final version of the manuscript.

**Notes**

The authors declare no competing financial interest.

## ■ REFERENCES

(1) Anastas, P.; Eghbali, N. Green Chemistry: Principles and Practice. *Chem. Soc. Rev.* **2010**, *39*, 301−312.

(2) Tortoioli, S.; Friedli, A.; Prud'homme, A.; Richard-Bildstein, S.; Kohler, P.; Abele, S.; Vilé, G. Development of an efficient and sustainable synthesis of 2-(3-methyl-1H-1,2,4-triazol-1-yl) acetic acid under continuous-flow conditions. *Green Chem.* **2020**, *22*, 3748−3758.

(3) Wurm, M.; Schöpke, B.; Lutz, D.; Müller, J.; Zeng, A.-P. Microtechnology meets systems biology: The small molecules of metabolome as next big targets. *J. Biotechnol.* **2010**, *149*, 33−51.

(4) Azuaje-Hualde, E.; García-Hernando, M.; Etxebarria-Elezgarai, J.; De Pancorbo, M.; Benito-Lopez, F.; Basabe-Desmonts, L. Microtechnologies for Cell Microenvironment Control and Monitoring. *Micromachines-Basel* **2017**, *8*, 166−186.

(5) Ou, X.; Chen, P.; Huang, X.; Li, S.; Liu, B. F. Microfluidic chip electrophoresis for biochemical analysis. *J. Sep. Sci.* **2020**, *43*, 258−270.

(6) Vaidyanathan, R.; Yeo, T.; Lim, C. T. Chapter 9 - Microfluidics for cell sorting and single cell analysis from whole blood. *Methods in Cell Biology*; Piel, M., Fletcher, D., Doh, J., Eds.; Academic Press, 2018; Vol. *147*, pp 151−173.

(7) Sackmann, E. K.; Fulton, A. L.; Beebe, D. J. The present and future role of microfluidics in biomedical research. *Nature* **2014**, *507*, 181−189.

(8) Lu, M.; Ozcelik, A.; Grigsby, C. L.; Zhao, Y.; Guo, F.; Leong, K. W.; Huang, T. J. Microfluidic hydrodynamic focusing for synthesis of nanomaterials. *Nano Today* **2016**, *11*, 778−792.

(9) Zizzari, A.; Carbone, L.; Cesaria, M.; Bianco, M.; Perrone, E.; Rendina, F.; Arima, V. Continuous flow scalable production of injectable size-monodisperse nanoliposomes in easy-fabrication milli-fluidic reactors. *Chem. Eng. Sci.* **2021**, *235*, 116481−116489.

(10) Wohlgemuth, R.; Plazl, I.; Žnidaršič-Plazl, P.; Gernaey, K. V.; Woodley, J. M. Microscale technology and biocatalytic processes: opportunities and challenges for synthesis. *Trends Biotechnol.* **2015**, *33*, 302−314.

(11) Dittrich, P. S.; Manz, A. Lab-on-a-chip: microfluidics in drug discovery. *Nat. Rev. Drug Discovery* **2006**, *5*, 210−218.

(12) Arima, V.; Pascali, G.; Lade, O.; Kretschmer, H. R.; Bernsdorf, I.; Hammond, V.; Watts, P.; De Leonardis, F.; Tarn, M. D.; Pamme, N.; Cvetkovic, B. Z.; Dittrich, P. S.; Vasovic, N.; Duane, R.; Jaksic, A.; Zacheo, A.; Zizzari, A.; Marra, L.; Perrone, E.; Salvadori, P. A.; Rinaldi, R. Radiochemistry on chip: Towards dose-on-demand synthesis of PET radiopharmaceuticals. *Lab Chip* **2013**, *13*, 2328−2336.

(13) Agustini, D.; Fedalto, L.; Bergamini, M. F.; Marcolino-Junior, L. H. Microfluidic thread based electroanalytical system for green chromatographic separations. *Lab Chip* **2018**, *18*, 670−678.

(14) Olives, A. I.; González-Ruiz, V.; Martín, M. A. Sustainable and Eco-Friendly Alternatives for Liquid Chromatographic Analysis. *ACS Sustain. Chem. Eng.* **2017**, *5*, 5618−5634.

(15) Marra, L.; Fusillo, V.; Wiles, C.; Zizzari, A.; Watts, P.; Rinaldi, R.; Arima, V. Sol-Gel Catalysts as an Efficient Tool for the Kumada-Corriu Reaction in Continuous Flow. *Sci. Adv. Mater.* **2013**, *5*, 475−483.

(16) Protasova, L. N.; Bulut, M.; Ormerod, D.; Buekenhoudt, A.; Berton, J.; Stevens, C. V. Latest Highlights in Liquid-Phase Reactions for Organic Synthesis in Microreactors. *Org. Process Res. Dev.* **2013**, *17*, 760−791.

(17) McQuade, D. T.; Seeberger, P. H. Applying Flow Chemistry: Methods, Materials, and Multistep Synthesis. *J. Org. Chem.* **2013**, *78*, 6384−6389.

(18) Neubauer, P.; Cruz, N.; Glauche, F.; Junne, S.; Knepper, A.; Raven, M. Consistent development of bioprocesses from microliter cultures to the industrial scale. *Eng. Life Sci.* **2013**, *13*, 224−238.

(19) Gutierrez, L.; Gomez, L.; Irusta, S.; Arruebo, M.; Santamaria, J. Comparative study of the synthesis of silica nanoparticles in micromixer−microreactor and batch reactor systems. *Chem. Eng. J.* **2011**, *171*, 674−683.

(20) Giorello, A.; Gioria, E.; Hueso, J. L.; Sebastian, V.; Arruebo, M.; Veaute, C.; Gutierrez, L. Natural polysaccharides and microfluidics: A win−win combination towards the green and continuous production of long-term stable silver nanoparticles. *J. Environ. Chem. Eng.* **2018**, *6*, 5069−5078.

(21) Zizzari, A.; Bianco, M.; Carbone, L.; Perrone, E.; Amato, F.; Maruccio, G.; Rendina, F.; Arima, V. Continuous-Flow Production of Injectable Liposomes via a Microfluidic Approach. *Materials* **2017**, *10*, 1411−1423.

(22) Carugo, D.; Bottaro, E.; Owen, J.; Stride, E.; Nastruzzi, C. Liposome production by microfluidics: potential and limiting factors. *Sci. Rep.* **2016**, *6*, 25876−25890.

(23) Zacheo, A.; Quarta, A.; Zizzari, A.; Monteduro, A. G.; Maruccio, G.; Arima, V.; Gigli, G. One step preparation of quantum dot-embedded lipid nanovesicles by a microfluidic device. *RSC Adv.* **2015**, *5*, 98576−98582.

(24) Dittrich, P. S.; Heule, M.; Renaud, P.; Manz, A. On-chip extrusion of lipid vesicles and tubes through microsized apertures. *Lab Chip* **2006**, *6*, 488−493.

(25) Kuroiwa, T.; Kiuchi, H.; Noda, K.; Kobayashi, I.; Nakajima, M.; Uemura, K.; Sato, S.; Mukataka, S.; Ichikawa, S. Controlled preparation of giant vesicles from uniform water droplets obtained by microchannel emulsification with bilayer-forming lipids as emulsifiers. *Microfluid. Nanofluid.* **2008**, *6*, 811−821.

(26) Nishimura, K.; Suzuki, H.; Toyota, T.; Yomo, T. Size control of giant unilamellar vesicles prepared from inverted emulsion droplets. *J.Colloid Interf. Sci.* **2012**, *376*, 119−125.

(27) Kastner, E.; Kaur, R.; Lowry, D.; Moghaddam, B.; Wilkinson, A.; Perrie, Y. High-throughput manufacturing of size-tuned liposomes by a new microfluidics method using enhanced statistical tools for characterization. *Int. J. Pharm.* **2014**, *477*, 361−368.

(28) Jahn, A.; Vreeland, W. N.; DeVoe, D. L.; Locascio, L. E.; Gaitan, M. Microfluidic Directed Formation of Liposomes of Controlled Size. *Langmuir* **2007**, *23*, 6289−6293.

(29) Jahn, A.; Stavis, S. M.; Hong, J. S.; Vreeland, W. N.; DeVoe, D. L.; Gaitan, M. Microfluidic Mixing and the Formation of Nanoscale Lipid Vesicles. *ACS Nano* **2010**, *4*, 2077−2087.

(30) Di Bello, M. P.; Bloise, E.; Mazzetto, S. E.; Mele, G. Formulation and Chemical Stability in Aqueous Media of Cannabidiol Embedded in Cardanol-Based Nanovesicles. *ACS Sustain. Chem. Eng.* **2017**, *5*, 8870−8875.

(31) Lomonaco, D.; Mele, G.; Mazzetto, S. E. Cashew Nutshell Liquid (CNSL): From an Agro-industrial Waste to a Sustainable Alternative to Petrochemical Resources. In *Cashew Nut Shell Liquid: A*

*Goldfield for Functional Materials*; Anilkumar, P., Ed.; Springer International Publishing: Cham, 2017; pp 19−38.

(32) Behalo, M. S.; Bloise, E.; Mele, G.; Salomone, A.; Messa, F.; Carbone, L.; Mazzetto, S. E.; Lomonaco, D. Bio-based benzoxazines synthesized in a deep eutectic solvent: A greener approach toward vesicular nanosystems. *J. Heterocyclic Chem.* **2020**, *57*, 768−773.

(33) De Maria, P.; Filippone, P.; Fontana, A.; Gasbarri, C.; Siani, G.; Velluto, D. Cardanol as a replacement for cholesterol into the lipid bilayer of POPC liposomes. *Colloids Surf., B* **2005**, *40*, 11−18.

(34) Yang, X. H.; Wang, Z. M.; Jing, F.; Hu, L. H.; Zhou, Y. H. A Brief Review of Cardanol-Based Surfactants. *Appl. Mech. Mater.* **2014**, *483*, 83−87.

(35) Balachandran, V. S.; Jadhav, S. R.; Vemula, P. K.; John, G. Recent advances in cardanol chemistry in a nutshell: from a nut to nanomaterials. *Chem. Soc. Rev.* **2013**, *42*, 427−438.

(36) Peungjitton, P.; Sangvanich, P.; Pornpakakul, S.; Petsom, A.; Roengsumran, S. Sodium Cardanol Sulfonate Surfactant from Cashew Nut Shell Liquid. *J. Surfactants Deterg.* **2009**, *12*, 85−89.

(37) Castro Dantas, T. N.; Vale, T. Y. F.; Dantas Neto, A. A.; Scatena, H., Jr.; Moura, M. C. P. A. Micellization study and adsorption properties of an ionic surfactant synthesized from hydrogenated cardanol in air-water and in air-brine interfaces. *Colloid Polym. Sci.* **2009**, *287*, 81−87.

(38) Anilkumar, P.; Jayakannan, M. Divergent Nanostructures from Identical Ingredients: Unique Amphiphilic Micelle Template for Polyaniline Nanofibers, Tubes, Rods, and Spheres. *Macromolecules* **2008**, *41*, 7706−7715.

(39) Anilkumar, P.; Jayakannan, M. Self-Assembled Cylindrical and Vesicular Molecular Templates for Polyaniline Nanofibers and Nanotapes. *J. Phys. Chem. B* **2009**, *113*, 11614−11624.

(40) Balachandran, V. S.; Jadhav, S. R.; Pradhan, P.; De Carlo, S.; John, G. Adhesive Vesicles through Adaptive Response of a Biobased Surfactant. *Angew. Chem., Int. Ed.* **2010**, *49*, 9509−9512.

(41) Przeworska, E.; Gubernator, J.; Kozubek, A. Formation of liposomes by resorcinolic lipids, single-chain phenolic amphiphiles from Anacardium occidentale L. *Biochim. Biophys. Acta, Biomembr.* **2001**, *1513*, 75−81.

(42) Bloise, E.; Carbone, L.; Colafemmina, G.; D'Accolti, L.; Mazzetto, S. E.; Vasapollo, G.; Mele, G. First Example of a Lipophilic Porphyrin-Cardanol Hybrid Embedded in a Cardanol-Based Micellar Nanodispersion. *Molecules* **2012**, *17*, 12252−12261.

(43) Needham, D.; Nunn, R. S. Elastic deformation and failure of lipid bilayer membranes containing cholesterol. *Biophys. J.* **1990**, *58*, 997−1009.

(44) Thewalt, J. L.; Bloom, M. Phosphatidylcholine: cholesterol phase diagrams. *Biophys. J.* **1992**, *63*, 1176−1181.

(45) Kaddah, S.; Khreich, N.; Kaddah, F.; Charcosset, C.; Greige-Gerges, H. Cholesterol modulates the liposome membrane fluidity and permeability for a hydrophilic molecule. *Food Chem. Toxicol.* **2018**, *113*, 40−48.

(46) Briuglia, M.-L.; Rotella, C.; McFarlane, A.; Lamprou, D. A. Influence of cholesterol on liposome stability and on in vitro drug release. *Drug Delivery Transl. Res.* **2015**, *5*, 231−242.

(47) Miao, Z.-L.; Deng, Y.-J.; Du, H.-Y.; Suo, X.-B.; Wang, X.-Y.; Wang, X.; Wang, L.; Cui, L.-J.; Duan, N. Preparation of a liposomal delivery system and its in vitro release of rapamycin. *Exp. Ther. Med.* **2015**, *9*, 941−946.

(48) Behalo, M. S.; Bloise, E.; Carbone, L.; Sole, R. D.; Lomonaco, D.; Mazzetto, S. E.; Mele, G.; Mergola, L. Cardanol-based green nanovesicles with antioxidant and cytotoxic activities. *J. Exp. Nanosci.* **2016**, *11*, 1274−1284.

(49) Bloise, E.; Di Bello, M. P.; Mele, G.; Rizzello, L. A green method for the production of an efficient bioimaging nanotool. *Nanoscale Adv.* **2019**, *1*, 1193−1199.

(50) Fontana, A.; Guernelli, S.; Zaccheroni, N.; Zappacosta, R.; Genovese, D.; De Crescentini, L.; Riela, S. Micellization properties of cardanol as a renewable co-surfactant. *Org. Biomol. Chem.* **2015**, *13*, 9214−9222.

(51) Pattni, B. S.; Chupin, V. V.; Torchilin, V. P. New Developments in Liposomal Drug Delivery. *Chem. Rev.* **2015**, *115*, 10938−10966.

(52) Amorati, R.; Pedulli, G. F.; Valgimigli, L.; Attanasi, O. A.; Filippone, P.; Fiorucci, C.; Saladino, R. Absolute rate constants for the reaction of peroxyl radicals with cardanol derivatives. *J. Chem. Soc., Perkin Trans. 2* **2001**, 2142−2146.

(53) Valenza, M.; Chen, J. Y.; Di Paolo, E.; Ruozi, B.; Belletti, D.; Ferrari Bardile, C.; Leoni, V.; Caccia, C.; Brilli, E.; Di Donato, S.; Boido, M. M.; Vercelli, A.; Vandelli, M. A.; Forni, F.; Cepeda, C.; Levine, M. S.; Tosi, G.; Cattaneo, E. Cholesterol-loaded nanoparticles ameliorate synaptic and cognitive function in H untington's disease mice. *EMBO Mol. Med.* **2015**, *7*, 1547−1564.

(54) Passoni, A.; Favagrossa, M.; Colombo, L.; Bagnati, R.; Gobbi, M.; Diomede, L.; Birolini, G.; Di Paolo, E.; Valenza, M.; Cattaneo, E.; Salmona, M. Efficacy of Cholesterol Nose-to-Brain Delivery for Brain Targeting in Huntington's Disease. *ACS Chem. Neurosci.* **2020**, *11*, 367−372.

(55) Al-Hazzani, A.; Periyasamy, V.; Subash-Babu, P.; Alshatwi, A. A. Formulation of cashew nut shell liquid (CSNL) nanoemulsion, a potent inhibitor of human MCF-7 breast cancer cell proliferation. *Med. Chem. Res.* **2012**, *21*, 1384−1388.

(56) Parasa, L. S.; Tumati, S.; Kumar, L.; Chigurupati, S. P.; Rao, G. S. In vitro antimicrobial activity of cashew (Anacardium occidentale, L.) nuts shell liquid against methicillin resistant staphylococcusaureus (MRSA) clinical isolates. *Int. J. Pharm. Pharm. Sci.* **2011**, *3*, 436−440.

(57) Teerasripreecha, D.; Phuwapraisirisan, P.; Puthong, S.; Kimura, K.; Okuyama, M.; Mori, H.; Kimura, A.; Chanchao, C. In vitro antiproliferative/cytotoxic activity on cancer cell lines of a cardanol and a cardol enriched from Thai Apis mellifera propolis. *BMC Complementary Altern. Med.* **2012**, *12*, 27.

(58) Zacheo, A.; Zizzari, A.; Perrone, E.; Carbone, L.; Giancane, G.; Valli, L.; Rinaldi, R.; Arima, V. Fast and safe microwave-assisted glass channel-shaped microstructure fabrication. *Lab Chip* **2015**, *15*, 2395−2399.

(59) Franken, L. E.; Boekema, E. J.; Stuart, M. C. A. Transmission Electron Microscopy as a Tool for the Characterization of Soft Materials: Application and Interpretation. *Adv. Sci.* **2017**, *4*, 1600476.

(60) Bello, V.; Mattei, G.; Mazzoldi, P.; Vivenza, N.; Gasco, P.; Idee, J. M.; Robic, C.; Borsella, E. Transmission Electron Microscopy of Lipid Vesicles for Drug Delivery: Comparison between Positive and Negative Staining. *Microsc. Microanal.* **2010**, *16*, 456−461.

(61) Fromherz, P. Lipid-vesicle structure: Size control by edge-active agents. *Chem. Phys. Lett.* **1983**, *94*, 259−266.

(62) Zook, J. M.; Vreeland, W. N. Effects of temperature, acyl chain length, and flow-rate ratio on liposome formation and size in a microfluidic hydrodynamic focusing device. *Soft Matter* **2010**, *6*, 1352−1360.

(63) Chen, Z.; Han, J. Y.; Shumate, L.; Fedak, R.; DeVoe, D. L. High Throughput Nanoliposome Formation Using 3D Printed Microfluidic Flow Focusing Chips. *Adv. Mater. Technol.* **2019**, *4*, 1800511.

(64) Phapal, S. M.; Sunthar, P. Influence of micro-mixing on the size of liposomes self-assembled from miscible liquid phases. *Chem. Phys. Lipids* **2013**, *172−173*, 20−30.

(65) McNaught, A. D.; Wilkinson, A. *IUPAC Compendium of Chemical Terminology*, 2nd ed.; Blackwell Science Publications: Oxford, 1997.

(66) Has, C.; Phapal, S. M.; Sunthar, P. Rapid single-step formation of liposomes by flow assisted stationary phase interdiffusion. *Chem. Phys. Lipids* **2018**, *212*, 144−151.

(67) Bottaro, E.; Nastruzzi, C. Off-the-shelf" microfluidic devices for the production of liposomes for drug delivery. *Mater. Sci. Eng., C* **2016**, *64*, 29−33.

(68) Falck, E.; Patra, M.; Karttunen, M.; Hyvönen, M. T.; Vattulainen, I. Lessons of Slicing Membranes: Interplay of Packing, Free Area, and Lateral Diffusion in Phospholipid/Cholesterol Bilayers. *Biophys. J.* **2004**, *87*, 1076−1091.

(69) Stuart, M. C. A.; Boekema, E. J. Two distinct mechanisms of vesicle-to-micelle and micelle-to-vesicle transition are mediated by the

packing parameter of phospholipid—detergent systems. *Biochim. Biophys. Acta, Biomembr.* **2007**, *1768*, 2681−2689.

(70) Kumar, V. V. Complementary molecular shapes and additivity of the packing parameter of lipids. *Proc. Natl. Acad. Sci. U.S.A* **1991**, *88*, 444−448.

(71) Wu, Y. G.; Tabata, M.; Takamuku, T. A Rayleigh light scattering study on mixing states of 2-propanol—water binary mixtures widely used as mobile phase in separation. *Talanta* **2001**, *54*, 69−77.

(72) Koynova, R.; Tenchov, B. Interactions of surfactants and fatty acids with lipids. *Curr. Opin. Colloid Interface Sci.* **2001**, *6*, 277−286.

(73) Cano-Sarabia, M.; Angelova, A.; Ventosa, N.; Lesieur, S.; Veciana, J. Cholesterol induced CTAB micelle-to-vesicle phase transitions. *J.Colloid Interf. Sci.* **2010**, *350*, 10−15.

(74) Lasic, D. D. On the thermodynamic stability of liposomes. *J.Colloid Interf. Sci.* **1990**, *140*, 302−304.

## 📖 Recommended by ACS